

# UCSF

## UC San Francisco Previously Published Works

### Title

Kinetic and structural investigations of novel inhibitors of human epithelial 15-lipoxygenase-2

### Permalink

<https://escholarship.org/uc/item/71k8s5jp>

### Authors

Tsai, Wan-Chen  
Gilbert, Nathan C  
Ohler, Amanda  
[et al.](#)

### Publication Date

2021-09-01

### DOI

10.1016/j.bmc.2021.116349

Peer reviewed



Published in final edited form as:

*Bioorg Med Chem.* 2021 September 15; 46: 116349. doi:10.1016/j.bmc.2021.116349.

## Kinetic and Structural Investigations of Novel Inhibitors of Human Epithelial 15-Lipoxygenase-2

Wan-Chen Tsai<sup>1</sup>, Nathaniel C. Gilbert<sup>2</sup>, Amanda Ohler<sup>3</sup>, Michelle Armstrong<sup>1</sup>, Steven Perry<sup>1</sup>, Chakrapani Kalyanaraman<sup>4</sup>, Adam Yasgar<sup>5</sup>, Ganesha Rai<sup>5</sup>, Anton Simeonov<sup>5</sup>, Ajit Jadhav<sup>5</sup>, Melissa Standley<sup>1</sup>, Hsiau-Wei Lee<sup>1</sup>, Phillip Crews<sup>1</sup>, Anthony T. Iavarone<sup>6</sup>, Matthew P. Jacobson<sup>4</sup>, David B. Neau<sup>7</sup>, Adam R. Offenbacher<sup>3</sup>, Marcia Newcomer<sup>2,\*</sup>, Theodore R. Holman<sup>1,\*</sup>

<sup>1</sup>Department of Chemistry and Biochemistry, University of California Santa Cruz, Santa Cruz, CA 95064, United States

<sup>2</sup>Department of Biological Sciences, Louisiana State University, Baton Rouge, LA, 70803, United States

<sup>3</sup>Department of Chemistry, East Carolina University, Greenville, North Carolina 27858

<sup>4</sup>Department of Pharmaceutical Chemistry, School of Pharmacy, University of California San Francisco, San Francisco, CA 94158, United States

<sup>5</sup>National Center for Advancing Translational Sciences, National Institutes of Health, 9800 Medical Center Drive, Rockville, Maryland 20850, United States

<sup>6</sup>Department of Chemistry and California Institute for Quantitative Biosciences (QB3), University of California Berkeley, Berkeley, California 94720, United States

<sup>7</sup>Cornell University, Northeastern Collaborative Access Team, Argonne National Laboratory, Argonne, IL, USA.

### Abstract

Human epithelial 15-lipoxygenase-2 (h15-LOX-2, ALOX15B) is expressed in many tissues and has been implicated in atherosclerosis, cystic fibrosis and ferroptosis. However, there are few reported potent/selective inhibitors that are active *ex vivo*. In the current work, we report newly discovered molecules that are more potent and structurally distinct from our previous inhibitors, **MLS000545091** and **MLS000536924** (Jameson et al, PLoS One, 2014, 9, e104094), in that they contain a central imidazole ring, which is substituted at the 1-position with a phenyl moiety and with a benzylthio moiety at the 2-position. The initial three molecules were mixed-type, non-reductive inhibitors, with IC<sub>50</sub> values of 0.34 ± 0.05 μM for **MLS000327069**, 0.53 ± 0.04 μM for **MLS000327186** and 0.87 ± 0.06 μM for **MLS000327206** and greater than 50-fold selectivity versus h5-LOX, h12-LOX, h15-LOX-1, COX-1 and COX-2. A small set of focused analogs was synthesized to demonstrate the validity of the hits. In addition, a binding model was developed for the three imidazole inhibitors based on computational docking and a co-structure of

\*Corresponding Author: Theodore R. Holman, Tel.: +1 831 459 5884; fax: +1 831 459 2935. holman@ucsc.edu.

Disclaimer: MPJ is a consultant to and shareholder of Schrodinger LLC, which licenses the software used in this work.

h15-LOX-2 with **MLS000536924**. Hydrogen/deuterium exchange (HDX) results indicate a similar binding mode between **MLS000536924** and **MLS000327069**, however, the latter restricts protein motion of helix- $\alpha$ 2 more, consistent with its greater potency. Given these results, we designed, docked, and synthesized novel inhibitors of the imidazole scaffold and confirmed our binding mode hypothesis. Importantly, four of the five inhibitors mentioned above are active in an h15-LOX-2/HEK293 cell assay and thus they could be important tool compounds in gaining a better understanding of h15-LOX-2's role in human biology. As such, a suite of similar pharmacophores that target h15-LOX-2 both *in vitro* and *ex vivo* are presented in the hope of developing them as therapeutic agents.

## Introduction

Lipoxygenases catalyze the peroxidation of fatty acids that contain bisallylic hydrogens between two *cis* double bonds, such as in linoleic acid (LA) and arachidonic acid (AA).<sup>1</sup> Lipoxygenases are named according to their product specificity with AA as the substrate because AA is the precursor of many active lipid metabolites that are involved in a number of significant disease states.<sup>2-4</sup> The human genome contains six functional human lipoxygenases (LOX) genes (ALOX5, ALOX12, ALOX12B, ALOX15, ALOX15B, eLOX3) encoding for six different human LOX isoforms (h5-LOX, h12-LOX, h12R-LOX, h15-LOX-1, h15-LOX-2, eLOX3, respectively).<sup>3</sup> The biological role in health and disease for each LOX isozyme varies dramatically, ranging from asthma (h5-LOX) to diabetes (h12-LOX) to stroke (h15-LOX-1).<sup>2</sup>

The role of epithelial h15-LOX-2 (ALOX15B) is not as clear as those of the other isozymes. h15-LOX-2 is expressed in macrophages, neutrophils, skin, hair roots, and prostate.<sup>5-7</sup> It is also highly expressed in atherosclerotic plaques and linked to the progression of macrophages to foam cells, which are present in atherosclerotic plaques.<sup>2, 7-11</sup> Recent data demonstrate that silencing the ALOX15B gene in human macrophages leads to decreased cellular lipid accumulation, a major factor in foam cell formation and thus plaque accumulation.<sup>12, 13</sup> Furthermore, h15-LOX-2 mRNA levels are highly elevated in human macrophages isolated from carotid atherosclerotic lesions of symptomatic rather than asymptomatic patients<sup>12, 14</sup> and its products have been shown to promote the formation of atherosclerotic lesions in a mouse model.<sup>15</sup>

Additionally, h15-LOX-2 has been shown to play a central role in the “class switch” of eicosanoid mediator biosynthesis from leukotrienes (LTs) to the anti-inflammatory and specialized pro-resolving mediator class of lipoxins (LXs) in the airways. The Urbach lab observed that the reduced expression level of h15-LOX-2 in the lower airways was associated with a depressed LXA<sub>4</sub>/LTB<sub>4</sub> ratio which contributed to cystic fibrosis (CF) lung disease in children.<sup>16</sup>

Furthermore, the h15-LOX-2/PEBP1 complex has been demonstrated to be a regulator of ferroptosis, with PEBP1 acting as a rheostat by changing h15-LOX-2 substrate specificity from free polyunsaturated fatty acids (PUFA) to PUFA-phosphatidylethanolamines (PE), leading to the generation of hydroperoxyeicosatetraenoic acid (HpETE) esterified into PE (HpETE-PE).<sup>17</sup> Accumulation of these hydroperoxy membrane phospholipids has been

shown to cause ferroptotic cell death, which implicates h15-LOX-2 in neurodegenerative diseases, such as Alzheimer's, Parkinson's and Huntington's diseases.<sup>18</sup>

The role of h15-LOX-2 in atherosclerosis, cystic fibrosis (CF), and ferroptosis implicate h15-LOX-2 as a potential therapeutic target for drug discovery, but currently, only a few published inhibitors targeting h15-LOX-2 have been reported (Figure 1). Nordihydroguaiaretic acid (NDGA), a redox inhibitor, has a potency of 11  $\mu\text{M}$ ,<sup>19</sup> and a 6,7-dihydroxyisoflavan (compound 27d) has an  $\text{IC}_{50} = 8 \mu\text{M}$ ,<sup>19</sup> but neither molecule is selective towards h15-LOX-2. Two molecules previously discovered by our laboratory, MLS000545091 (**545091**) and MLS000536924 (**536924**), do exhibit strong potency, as well as selectivity for h15-LOX-2, with  $\text{IC}_{50}$  values of 2.6 and 3.1  $\mu\text{M}$ , respectively.<sup>20</sup> The observed micromolar potencies of these inhibitors in biochemical assays constitute acceptable probe molecule criteria for h15-LOX-2 inhibition, but it is unknown if these molecules potentially inhibit h15-LOX-2 in cells, which would enable further interrogation in advanced disease models. The lack of cellular activity investigations, as well as the dearth of h15-LOX-2 inhibitor chemotypes, underscore the importance of discovering additional inhibitors and determining their *ex vivo* activity so they could be used to probe the role of h15-LOX-2 in atherosclerosis, cystic fibrosis (CF) lung disease and ferroptosis models. Herein, we report the discovery and characterization of a novel chemotype that is potent and selective against h15-LOX-2. In addition, there are currently no co-structures of inhibitors bound to h15-LOX-2. In the current paper, we identify the chemotype binding mode with computer docking models, a crystallographic co-structure, and hydrogen/deuterium exchange (HDX) investigations, which provide proof-of-principle for future structure-activity relationship (SAR)/drug design efforts to target h15-LOX-2.

## 2. Materials and Methods

### 2.1 Materials

All commercial fatty acids were purchased from Nu Chek Prep, Inc. (MN, USA). BWb70c was purchased from Sigma/Aldrich Chemicals. Unless specifically mentioned, the inhibitors were obtained from the NIH Molecular Libraries Small Molecule Repository (MLSMR): (<https://mli.nih.gov/mli/compound-repository/>). All other chemicals were reagent grade or better and were used without further purification.

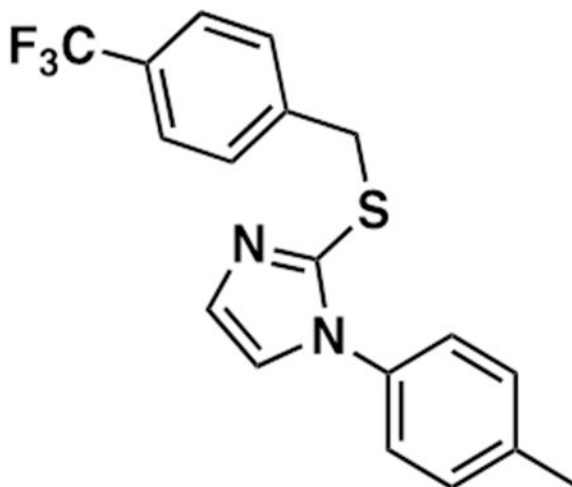
### 2.2 Inhibitor Synthesis

**General Methods for Chemistry**—All air or moisture-sensitive reactions were performed under a positive pressure of nitrogen with oven-dried glasswares. Chemical reagents and anhydrous solvents were obtained from commercial sources and used as-is. The purity of the compounds was greater than 95% and  $^1\text{H}$  and  $^{13}\text{C}$  NMR spectra were recorded on a Bruker Avance III HD 500MHz NMR spectrometer. The novel inhibitors were synthesized via the steps shown in Scheme 1.

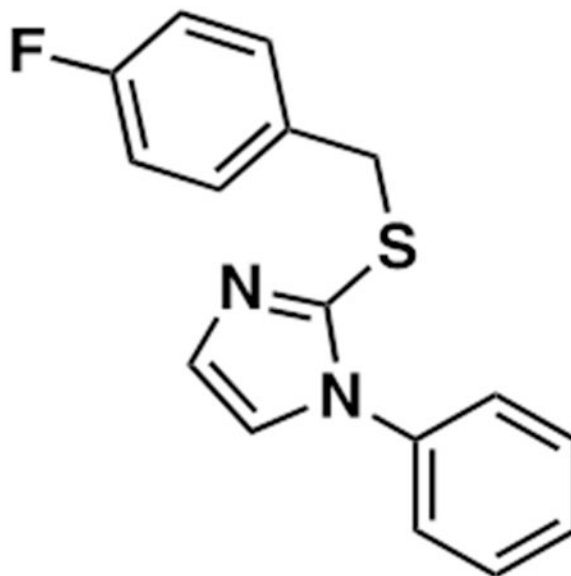
**Step 1.** A mixture of required phenyl isothiocyanate (5 mmol) and aminoacetaldehyde diethyl acetal (5 mmol) in toluene (10 mL) was stirred at room temperature for 1 h. To the reaction mixture, conc. HCl (37 wt. % in water, 2.5 mmol) was added, followed by heating

to reflux (bath temp. = 110° C) for 1-3 h. After evaporating the solvents, the residue was treated with water and 1N NaOH (the pH was set to 8). The precipitates were collected by filtration, washed with water and hexane/ether, and dried in a vacuum to give the desired imidazole-2-thiol products, which were recrystallized from an appropriate solvent (acetonitrile, methanol, or benzene) (yield: 43-53%).

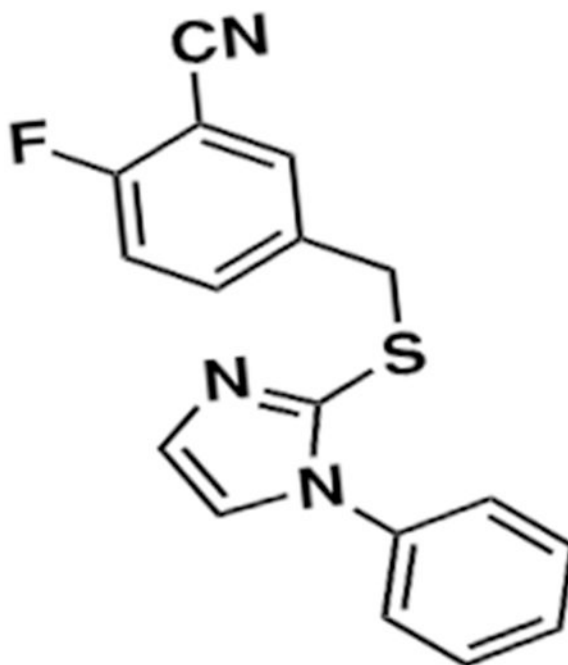
**Step 2.** Imidazole-2-thiol product from step 1 (5 mmol) in acetone was placed in the flask and potassium carbonate (15 mmol) was slowly added. The reaction was stirred under nitrogen for 1 h and then benzyl bromide (7.5 mmol) in ethanol (10 mL) was added. The reaction was heated to 80° C for 12 h. After removal of the solvent, the residue was purified by normal phase silica chromatography (DCM/MeOH = 4/1) to get desired final product. (yield: 60-69%)



**1-(*p*-tolyl)-2-((4-(trifluoromethyl)benzyl)thio)-1*H*-imidazole (1):** <sup>1</sup>H NMR (500 MHz, CDCl<sub>3</sub>) δ 7.37 (d, 2H), 7.20 (d, 2H), 7.11 (s, 1H), 7.09 (d, 2H), 6.97 (s, 1H), 6.89 (d, 2H), 4.19 (s, 2H), 2.30 (s, 3H). <sup>13</sup>C NMR (500 MHz, CD<sub>3</sub>OD) δ 141.8, 140.9, 138.5, 134.5, 129.8, 129.7, 129.2, 125.3, 122.8, 38.3, 21.2. HRMS *m/z* 348.0909 [M<sup>+</sup>] (calculated for C<sub>18</sub>H<sub>15</sub>F<sub>3</sub>N<sub>2</sub>S, 348.0908). See Supporting information, Figures S1-3.



**2-((4-fluorobenzyl)thio)-1-phenyl-1H-imidazole (2):**  $^1\text{H}$  NMR (500 MHz,  $\text{CDCl}_3$ )  $\delta$  7.34 (m, 1H), 7.34 (d, 2H), 7.15 (s, 1H), 7.10 (d, 2H), 7.09 (d, 2H), 7.03 (s, 1H), 6.83 (t, 2H), 4.20 (s, 2H).  $^{13}\text{C}$  NMR (500 MHz,  $\text{CDCl}_3$ )  $\delta$  162.1, 141.5, 137.0, 132.9, 130.6, 129.5, 129.2, 125.6, 122.5, 115.3, 38.0. HRMS  $m/z$  284.0780 [ $\text{M}^+$ ] (calculated for  $\text{C}_{16}\text{H}_{13}\text{FN}_2\text{S}$ , 284.0783). See Supporting information, Figures S4-6.



**2-fluoro-5-(((1-phenyl-1H-imidazol-2-yl)thio)methyl)benzonitrile (3):**  $^1\text{H}$  NMR (500 MHz,  $\text{CDCl}_3$ )  $\delta$  7.37 (m, 5H), 7.11 (s, 1H), 7.11 (m, 2H), 7.04 (s, 1H), 6.98 (s, 1H), 4.15 (s, 2H).  $^{13}\text{C}$  NMR (500 MHz,  $\text{CDCl}_3$ )  $\delta$  161.4, 140.4, 136.9, 135.2, 133.3, 129.9, 129.3, 125.6,

122.8, 116.5, 113.7, 101.5, 36.9. HRMS  $m/z$  309.0737 [ $M^+$ ] (calculated for  $C_{17}H_{12}FN_3S$ , 309.0736). See Supporting information, **Figures S7-9**.

### 2.3 Protein Expression

h5-LOX,<sup>21</sup> h12-LOX,<sup>22</sup> h15-LOX-1<sup>22</sup> and h15-LOX-2<sup>19</sup> were expressed/purified as published and ovine COX-1 and Ovine COX-2 isozymes being purchased from Cayman Chemicals. Mouse 15-LOX-2 (m15-LOX-2) was expressed as follows. A plasmid containing the N-terminal His<sub>6</sub>-tagged m15-LOX-2 gene under the control of a T7 promoter sequence were transformed into Rosetta2 E. coli cells via heat shock.<sup>23</sup> A colony was grown in 2 mLs with Ampicillin/Chloramphenicol at 37° C for approximately 10 hours. The two mLs were added to 50 mLs of Enpresso media in UltraYield flasks with Air-O-top seals, according to the manufacturers instructions, and grown at 30° C for 24 hours. At this point, an Enpresso “booster” tablet was added with 1 mM IPTG and the cells grown an additional 24 hours at 20° C. Cells were harvested by centrifugation and lysed with a French pressure cell in 35 mL of 25 mM HEPES, 150 mM NaCl, 0.1% Triton X-100 (pH 7.5). The lysate was loaded onto a Ni-NTA column, washed with 3 column volumes of Buffer A (25 mM HEPES, 150 mM NaCl (pH 7.5)), and eluted with a step-gradient of 25 mM HEPES, 150 mM NaCl, 250 mM imidazole (pH 7.5). For h15-LOX-1, h15-LOX-2 and h12-LOX, they were also expressed as N-terminal His<sub>6</sub>-tagged proteins and purified via immobilized metal affinity chromatography (IMAC) using Ni-NTA resin, as published.<sup>22,19</sup> The purity of each protein was analyzed by SDS-PAGE and found to be greater than 90%. Human leukocyte 5-lipoxygenase was expressed as a non-tagged protein and used as a crude ammonium sulfate precipitated protein, as published.<sup>21</sup>

### 2.4 Lipoxygenase UV-Vis-based IC<sub>50</sub> Assay

The initial one-point inhibition percentages were determined by following the formation of the conjugated diene product at 234 nm ( $\epsilon = 25,000 \text{ M}^{-1}\text{cm}^{-1}$ ) with a Perkin-Elmer Lambda 40 UV/Vis spectrophotometer at 25  $\mu\text{M}$  inhibitor concentration. All inhibitors that showed greater than 70% inhibition were investigated further to determine their IC<sub>50</sub> values. The full IC<sub>50</sub> experiments were done with at least five different inhibitor concentrations. All reaction mixtures were 2 mL in volume and constantly stirred using a magnetic stir bar at room temperature (23°C) with the appropriate amount of LOX isozyme [h5-LOX (~ 200 nM); h12-LOX (~ 50 nM); h15-LOX-1 (~ 60 nM); h15-LOX-2 (~ 200 nM)]. The protein concentrations are the total protein concentration; however, active protein concentration will be significantly less due to incomplete metalation. Reactions with h12-LOX were carried out in 25 mM HEPES (pH 8.0) 0.01% Triton X-100 and 10  $\mu\text{M}$  AA. Reactions with the crude, ammonium sulfate precipitated h5-LOX were carried out in 25 mM HEPES (pH 7.3), 0.3 mM CaCl<sub>2</sub>, 0.1 mM EDTA, 0.2 mM ATP, 0.01% Triton X100 and 10  $\mu\text{M}$  AA. Reactions with h15-LOX-1 and h15-LOX-2 were carried out in 25 mM HEPES buffer (pH 7.5), 0.01% Triton X-100 and 10  $\mu\text{M}$  AA. The concentration of AA was quantitated by allowing the enzymatic reaction to proceed to completion in the presence of soybean 15-LOX-1 (s15-LOX-1). IC<sub>50</sub> values were obtained by determining the percent inhibition at various inhibitor concentrations and plotting against inhibitor concentration, followed by a hyperbolic saturation curve fit. The percent inhibition was calculated by comparing the enzymatic rate of the control (DMSO) to the enzymatic rate with the respective inhibitor

present. The experiments used for generating the saturation curves were performed in duplicate or triplicate, depending on the quality of the data. All inhibitors were stored at  $-20\text{ }^{\circ}\text{C}$  in DMSO.

## 2.5 Steady-State Inhibition Kinetics of h15-LOX-2

The steady-state equilibrium constants of dissociation for MLS000327069 (**327069**), MLS000327186 (**327186**), MLS000327206 (**327206**) were determined by monitoring the formation of the conjugated product, 15-HpETE, at 234 nm ( $\epsilon = 25,000\text{ M}^{-1}\text{cm}^{-1}$ ) with a Perkin Elmer Lambda 40 UV/Vis spectrophotometer. Reactions were initiated by adding enzyme to a constantly stirring 2 mL reaction mixture containing  $0.7\text{ }\mu\text{M} - 20\text{ }\mu\text{M}$  AA in 25 mM HEPES buffer (pH 7.5), in the presence of 0.01% Triton X-100. Kinetic data were obtained by recording initial enzymatic rates, at varied inhibitor concentrations, and subsequently fitting the data to the Henri-Michaelis-Menten equation using KaleidaGraph (Synergy) to determine  $V_{\text{max}}$  ( $\mu\text{mol}/\text{min}$ ) and  $K_{\text{m}}$  ( $\mu\text{M}$ ). The primary data were then plotted in Dixon format using Microsoft Excel by graphing  $1/v$  vs.  $[I]$   $\mu\text{M}$  at the chosen substrate concentrations. From the Dixon plots, the slope at each substrate concentration was extracted and plotted against  $1/[S]$   $\mu\text{M}$  to produce the Dixon replots. The  $K_{\text{ic}}$  equilibrium constant of dissociation was calculated by dividing  $K_{\text{m}} / V_{\text{max}}$  by the slope of the replot. To obtain  $K_{\text{iu}}$ ,  $1 / V_{\text{max}}$  was divided by the y-intercept of the replot.  $K_{\text{ic}}$  and  $K_{\text{iu}}$  are defined as the equilibrium constant of dissociation from the catalytic and secondary sites, respectively.

## 2.6 Pseudo-peroxidase Assay

The pseudo-peroxidase activity of **327069**, **327186**, **327206** was determined with h15-LOX-2 on a Perkin-Elmer Lambda 40 UV/Vis spectrophotometer as described previously.<sup>24</sup> 13-HpODE was used as the oxidant and BWb70c as the positive control. The reaction was initiated by addition of  $20\text{ }\mu\text{M}$  13-HpODE to 2 mL buffer (50 mM sodium phosphate (pH 7.4), 0.3 mM  $\text{CaCl}_2$ , 0.1 mM EDTA, 0.01% Triton X-100) containing  $20\text{ }\mu\text{M}$  **327069**, **327186**, or **327206** and 200 nM h15-LOX-2. The reaction mixtures were constantly stirred at  $23\text{ }^{\circ}\text{C}$ . The activity was determined by monitoring the decrease at 234 nm (product degradation) and the percent consumption of 13-HpODE was recorded. More than 25% 13-HpODE degradation indicates redox activity of that particular inhibitor. The negative controls used were: enzyme alone with the product, enzyme alone with inhibitor, as well as inhibitor alone with the product. These formed a baseline for the assay, reflecting non-pseudo-peroxidase dependent hydroperoxide product decomposition. To rule out the auto-inactivation of the enzyme from pseudo-peroxidase cycling, the h15-LOX-2 residual activity was determined by the addition of  $20\text{ }\mu\text{M}$  AA at the end of each reaction. The initial rates of the inhibitor and 13-HpODE were compared to the initial rates of inhibitor alone because the inhibitor by itself inherently lowers the rate of oxygenation. Activity is characterized by direct measurement of the product formation with the increase of absorbance at 234 nm.

## 2.7 Cyclooxygenase Selectivity Assay

Cyclooxygenase selectivity assay was performed as previously described.<sup>25</sup> Approximately  $3\text{ }\mu\text{g}$  of either ovine cyclooxygenase-1 (COX-1, PTGS1) or human recombinant cyclooxygenase-2 (COX-2, PTGS2) (Cayman Chemical) was added to buffer containing



0.1 M Tris-HCl buffer (pH 8.0), 5 mM EDTA, 2 mM phenol, and 1  $\mu$ M hemin at 37 °C. The selected inhibitors, **327069**, **327186**, or **327206**, were added to the reaction cell, followed by a 5-minute incubation with either of the COX isozymes. The reaction was then initiated by adding approximately 100  $\mu$ M AA in the reaction cell, as indicated in the enzymatic protocol (Cayman Chemicals). A Hansatech DWI oxygen electrode was utilized for data collection and the consumption of oxygen was recorded. Indomethacin and the vehicle of inhibitor (DMSO) were the positive and negative controls, respectively. The percent inhibition of the enzyme was calculated by comparing the rates of O<sub>2</sub> consumption for experimental samples (with inhibitor) to the rates of control samples (with DMSO).

## 2.8 Study of Inhibitors as Substrates

The inhibitors **327069**, **327186**, or **327206** were reacted with h15-LOX-2 to determine if they act as substrates. All buffer conditions and the determination of each rate were identical to the UV-Vis assay mentioned above (Methods section 2.4). 20  $\mu$ M of each inhibitor was reacted with h15-LOX-2 in 2-mL reaction mixtures in the absence of AA. Controls consisted of DMSO (vehicle), 10  $\mu$ M AA, and enzyme. All reactions were conducted on a Perkin Elmer Lambda 40 UV/Vis spectrophotometer. No change of absorbance at 234 nm or 280 nm was observed for each reaction. Each reaction mixture was subsequently extracted and analyzed via RP-HPLC using a Higgins HAsiL analytical column. Solution A was 99.9% ACN and 0.1% acetic acid; solution B was 99.9% H<sub>2</sub>O and 0.1% acetic acid. An isocratic elution of 55%A:45%B was used in the HPLC analysis. Retention times and absorbance spectra of each of the reactions were compared to spectra of the controls. Collectively, the data from the UV-Vis experiments as well as the HPLC analysis confirm that these inhibitors do not act as substrates to h15-LOX-2.

## 2.9 Virtual Screening of Novel h15-LOX-2 Inhibitors

Virtual screening software, Glide (version 8.7, Schrodinger Suite 2020 release 2), was used to predict the binding modes of the ligands **327069**, **327186** and **327206**. The structure of h15-LOX2 co-crystallized with a substrate mimic inhibitor (hydroxyethoxytri(ethoxy)octane) was used in Glide docking (pdb id: 4NRE). Prior to docking, the protein structure was subjected to a protein-preparation step (Schrodinger Inc). During this step, appropriate bond-orders and atom types were set, hydrogen atoms were added, protonation states of titratable residues such as His, Asp and Glu were adjusted, side chains of Asn, Gln, Thr and Tyr residues were optimized to make hydrogen bond interactions and, finally, a short minimization of the whole protein structure was performed such that the heavy atoms did not move beyond 0.3 Å from their starting positions. During the protein preparation step, we retained the co-crystallized ligand, the metal ion (Fe<sup>2+</sup>) and a water molecule that coordinates to the metal ion. The structures of the ligands identified in this study were built using the Edit/Build panel of Maestro software (version 12.4, Schrodinger Inc). They were subsequently energy minimized using LigPrep software (Schrodinger Inc). The docking process consisted of grid preparation and ligand-docking steps. After the protein-preparation step, we removed the co-crystallized ligand from protein-ligand complex structure and used its coordinates to define the docking-grid box center. Inhibitors were docked using the standard-precision (SP) docking scoring function. Initial attempts to dock the inhibitors using flexible-ligand rigid-receptor docking protocol, the docking program failed to identify

docking poses free of steric clashes for all three inhibitors. Therefore, we decided to treat both inhibitor and receptor flexibly by means of InducedFit docking, following our earlier work in which we successfully docked the h15-LOX-2 inhibitors, MLS000545091 (**545091**) and MLS000536924 (**536924**), after opening the active site using the InducedFit docking (InducedFit Dock, Schrodinger Inc).<sup>20</sup> During the InducedFit docking all residues in the active site, other than the Fe<sup>3+</sup>, the water molecule, and the metal-coordinating His373, His378 and His553, were treated flexibly. We took the protein model from the top ranking InducedFit docking pose for **327069** and then docked all inhibitors using standard rigid-receptor flexible ligand docking (Glide) with the standard-precision (SP) scoring function.

## 2.10 Co-Structure of h15-LOX-2 and Inhibitor

The loop mutant (LM) of h15-LOX-2 has amino acids 73-79 deleted (PPVLPLL) and was previously cloned and described.<sup>23</sup> Briefly, 15-LOX-2 LM is overexpressed in Rosetta 2 (DE3) cells in the pET Duet-1 vector with the *E. coli yjgD* gene after promoter 2. For the catalytically inactive Mn<sup>2+</sup>-substituted h15-LOX-2, the bacterial culture was grown in M9 minimal media containing 0.4% (w/v) glucose, 1 mM MgSO<sub>4</sub>, 0.1 mM CaCl<sub>2</sub>, 100 µg mL<sup>-1</sup> thiamine, 150 µM Mn(II)(SO<sub>4</sub>)<sub>2</sub>, and 0.2% (w/v) casamino acids. Enzyme was purified with a 5-mL Co<sup>2+</sup>-HisTrap HP column installed on an AKTA FPLC (Cytiva, formerly GE Healthcare Life Sciences). After the protein is bound, the column is washed with 20 column volumes (CV) of buffer A (20 mM Tris, 500 mM NaCl, 20 mM imidazole, pH 8.0) and eluted with a 20-CV gradient with buffer B (20 mM Tris, 500 mM NaCl, 200 mM imidazole, pH 8.0). Fractions are concentrated in Amicon Ultra-15 centrifugal filter units with a 30-kDa cutoff. Protein is applied to a Superdex 200 10/300 GL column; monomer and dimer peaks are collected and used separately for crystallization studies.

h15-LOX-2 LM Mn<sup>2+</sup>-substituted at 10 mg/mL with a cocktail of 500 µM of both inhibitors **545091** and **536924** was screened with sparse matrix screens from Hampton Research, Rigaku Reagents, Qiagen, and Molecular Dimensions on a Gryphon liquid dispenser (ARI). The condition of 20% Jeffamine M-2070 and 20% DMSO resulted in rod-like crystals directly from the HTS conditions. Attempts at repeating conditions by hand were unsuccessful. Jeffamine M-2070 is an industrial-grade reagent that was sold by Molecular Dimensions and is no longer available for purchase.

The h15-LOX-2 LM crystals were directly looped from the HTS condition and plunged into liquid N<sub>2</sub> for shipping. X-ray data were collected at the 24ID-E beamline of the Northeastern Collaborative Access Team at the Advanced Photon Source (Argonne National Laboratory). XDS, pointless, and Scala were used via the RAPD processing suite of the Northeastern Collaborative Access team. RAPD applies a resolution cutoff at  $CC_{1/2} > 0.35$ .<sup>26</sup> Molecular replacement with h15-LOX-2 (4NRE) was performed in the Phenix program suite and two molecules were placed in the asymmetric unit.<sup>27</sup> Phenix.refine and coot were used for refinement and manual model building. Phenix.elbow was used to generate restraints for the small molecule inhibitors. Density consistent with an inhibitor is present in the active site of both protomers in the asymmetric unit. However, given the similarity of the structures of the two compounds, it is not possible to determine if there is a mixture of occupancy for the inhibitors or a single inhibitor, and which orientation each inhibitor binds in the active

sites. Final refinements for each inhibitor positioned in the two possible binding modes in the electron density for each chain are included in the table below. The electron density clearly suggests that the inhibitor does not occupy a position in the metal coordination sphere. A water molecule mediates an interaction in chain A between the ligand and the metal. Real-space correlation coefficients and occupancies are provided in the final parallel refinements for both inhibitors in each chain and each orientation (Table 1).

## 2.11 Hydrogen/Deuterium Exchange-Mass Spectrometry of h15-LOX-2

Aliquots of 15-LOX-2, purified from *E. coli* cultures as described previously,<sup>8</sup> were thawed and were diluted 10-fold (5  $\mu$ L into 45  $\mu$ L) in 10 mM HEPES, 150 mM NaCl, pD 7.4 D<sub>2</sub>O (99%D, Cambridge Isotope Laboratories) buffer (corrected; pD = pH<sub>read</sub> + 0.4). Samples were incubated randomly at 10 time points (0, 10, 20, 45, 60, 180, 600, 1800, 3600, and 7200 s) at 25 °C using a water bath. For each given temperature and mutant, the time points (samples) were collected over the course of three to four days and randomized to reduce systematic error. Each sample (from a unique time point) was prepared and processed once. For the samples containing inhibitors, the inhibitor was added (20  $\mu$ M final concentration) to the protein stock solution (at least one minute) prior to D<sub>2</sub>O addition. The specific inhibitor was also added to the D<sub>2</sub>O buffer at a final concentration of 20  $\mu$ M prior to the exchange experiment.

Upon completion of the designated incubation time, all samples were then treated identically; the samples were rapidly cooled (5-6 seconds in a -20 °C bath) and acid quenched (to pH 2.4, confirmed with pH electrode, with 0.32 M citric acid stock solution [90 mM final concentration] at 0 °C). Procedures from this point were conducted near 4 °C. Prior to pepsin digestion, guanidine HCl (in citric acid, pH 2.4) was mixed with the samples to a final concentration of ca. 0.5 M. This solution contained DTT at the final concentration of 5 mM. The addition of the reducing and chaotropic agents was necessary for obtaining high coverage of the primary sequence (90-94%). 15-LOX-2 samples were digested with pre-equilibrated (10 mM citrate buffer, pH 2.4), immobilized pepsin for 2.5 min. The peptide fragments were filtered, and the pepsin was removed, using spin cups (cellulose acetate) and by centrifugation for 10 seconds at 4 °C. Samples were flash-frozen immediately in liquid nitrogen and stored at -80 °C until data collection.

Deuterated, pepsin-digested samples of 15-LOX-2 were analyzed using a 1200 series liquid chromatography system (Agilent, Santa Clara, CA) that was connected in line with an LTQ Orbitrap XL mass spectrometer (Thermo Fisher Scientific, Waltham, MA), as described by our laboratory previously (see Supporting Information for more details). Mass spectral data acquired for HDX measurements were analyzed using the software, HDX WorkBench.<sup>28</sup> The percent deuterium incorporation was calculated for each of these peptides, taking into account the number of amide linkages (excluding proline residues) and the calculated number of deuterons incorporated. The values were normalized for 100% D<sub>2</sub>O and corrected for peptide-specific back-exchange, HDX% = (observed, normalized extent of deuterium incorporation {in percent})/(1-{BE/100}).<sup>29, 30</sup> Back-exchange values ranged from 17 to 60%, for an average value of 36% (Supporting Information, HDX Table). The resulting data

were plotted as deuterium exchange versus time using Igor Pro software (See Supporting Information, HDX traces).

### 2.12 Inhibition of h15-LOX-2 in HEK293T cells

HEK293T cells over-expressing h15-LOX-2 were grown in minimum essential medium (MEM, Gibco) with 10% fetal bovine serum (FBS, Gibco), 2 mM glutamine (Sigma), 100 U/mL of penicillin/streptomycin (Gibco) and 640 ug/ml G418 sulfate (Fisher) as a selection agent. Cells were harvested at 90% confluence with trypsin-EDTA (Gibco) and washed once with MEM with 10% FBS. Cells were then washed with 0.1% glucose (Fisher) in PBS (Gibco). Cells were then diluted in 0.1% glucose in PBS to a concentration of 1 million cells/mL. Cells were treated with DMSO (0.2%) or inhibitor in DMSO and incubated at 37 °C for 20 min. Cells were then stimulated with 100  $\mu$ M CaCl<sub>2</sub> (Sigma), 5  $\mu$ M Ca Ionophore A23187 (Sigma), and 1  $\mu$ M arachidonic acid (NuCheck) for 10 min at 37 °C. Cells were then acidified to 40  $\mu$ M HCl and snap-frozen in liquid nitrogen. Analysis of 15-hydroxyeicosatetraenoic acid (15-HETE) was performed as described previously,<sup>31</sup> with the addition that MS/MS *m/z* transition 319.2→219 was used to measure 15-HETE. Leftover cells from the inhibition assay were used to seed flasks and grew as well as untreated cells. Additionally, a cell survival assay was performed, in which cells were treated with 0.2% DMSO, 10  $\mu$ M inhibitor, or 20  $\mu$ M inhibitor for 1 h. After incubation, the media was replaced, and the cells were monitored daily to assess cell death.

## 3. Results and Discussion

### 3.1 Compound Identification and Inhibitor Potency

Previously, our laboratory reported the identity of two novel, potent and specific h15-LOX-2 inhibitors, **545091** and **536924**, from our quantitative High Throughput Screening (qHTS) of a 107,261 compound library using our LOX assay.<sup>20</sup> Structurally, **545091** contains a 1,3,4-oxadiazole heterocycle, while **536924** contains a 1,2,4-triazole ring. These two inhibitors were discovered from manually screening the top 300 molecules of the qHTS using our LOX assay which determined micromolar potencies (Table 2). In the current work, the next top 600 molecules from the MLSMR were manually screened using our LOX assay, and three additional inhibitors were discovered, **327069**, **327186**, and **327206**. The newly discovered molecules are structurally different from **545091** and **536924** in that they contain a central imidazole ring, which is substituted at the 1-position with a phenyl moiety and with a benzylthio moiety at the 2-position (Table 2). In our *in vitro* LOX assay, **327069** inhibited h15-LOX-2 with an IC<sub>50</sub> of 0.34 ± 0.05  $\mu$ M, **327186** had a potency of 0.53 ± 0.04  $\mu$ M and **327206** showed a similar potency of 0.87 ± 0.06  $\mu$ M.

### 3.2 Steady-State Inhibition Kinetics

Given that **327069**, **327186**, and **327206** exhibited potency against h15-LOX-2, their modes of inhibition were probed utilizing steady-state inhibition kinetics. The formation of 15-HpETE was monitored as a function of substrate and inhibitor concentration in the presence of 0.01% Triton-X-100. Fitting the data for **327186** yielded mixed-type inhibition with a  $K_{ic}$  of 0.80 ± 0.05  $\mu$ M and a  $K_{iu}$  of 4.0 ± 3  $\mu$ M, which are defined as the equilibrium constants of inhibitor dissociation from the enzyme and enzyme-substrate complex, respectively

(Supporting Information, Figure S10). The steady-state inhibition kinetic experiments were also performed for **327069** and **327206** (Table 3), with the inhibition constants of all three molecules being comparable, as determined from their Dixon plots and Dixon replots. The data demonstrate that all three inhibitors exhibit mixed inhibition against h15-LOX-2, with the trends in the inhibition equilibrium constants being consistent with the IC<sub>50</sub> values (Table 2).

### 3.3 Selectivity inhibition assay with human LOX isozymes, m15-LOX-2 and COX-1/2.

Once the potencies of the three newly discovered small molecule inhibitors against h15-LOX-2 had been determined, their selectivity against LOX and COX isozymes was investigated. All three molecules displayed high selectivity, at least 50-fold, for h15-LOX-2 versus h15-LOX-1, h12-LOX, h5-LOX, COX-1 and COX-2 (Table 4). In addition, these inhibitors were tested against the m15-LOX-2, but unfortunately minimal activity was observed, indicating limited usefulness in mouse models which target m15-LOX-2.

### 3.4 Pseudo-Peroxidase Activity Assay

To better understand the mechanism of inhibition between **327069**, **327186**, and **327206** and h15-LOX-2, the redox capability of the three molecules was investigated in a pseudo-peroxidase activity assay. Although many LOX inhibitors in the literature exhibit redox activity, they are not regarded as good therapeutics due to their tendencies for off-target redox reactions. All three inhibitors were tested using the UV-Vis pseudo-peroxidase assay, with the lack of degradation of 13-HpODE at 234 nm confirming that the inhibitors are not redox-active (Table 4).

### 3.5 Substrate Activity of Inhibitor

To determine whether h15-LOX-2 can catalytically modify the inhibitors, 20 μM of each inhibitor was reacted with h15-LOX-2 and the reaction monitored at 205 nm, 234 nm and 280 nm. An increase in absorbance at each wavelength was not detected indicating no chemical reaction. To confirm these results, the reactions were extracted, dried under N<sub>2</sub> and brought up in methanol for RP-HPLC analysis. No significant difference in spectra or retention time was observed at 212 nm ( $\lambda_{\text{max}}$  of inhibitor), 234 nm or 280 nm, confirming that **327069**, **327186**, and **327206** are not substrates to h15-LOX-2.

### 3.6 Structure/Activity Relationship (SAR) Study

A comprehensive SAR exploration is beyond the scope of this manuscript but will be followed up in later manuscripts. Following the discovery of the new chemotype, a limited SAR was performed to demonstrate the validity of the hits utilizing both syntheses of the analogs and sourcing from commercial vendors (Supporting Information, Figure S11). **327069**, **327186**, and **327206** possess 3 different substituents at the para position of the benzylthio moiety, a trifluoromethyl (**327069**), a bromo (**327186**), and an ethyl (**327206**) moiety, all of which demonstrated comparable potency (Table 2). To probe the structure-activity relationship further, we prepared additional analogs containing variations on the benzylthio and *N*-phenyl moieties. From the aggregate data (Figure S11), we did not observe a clear SAR trend from our limited structural modifications, though most of the

similar analogs showed lower or comparable potencies to the original hits. Surprisingly, analog **2** with a *p*-fluoro group showed no activity up to 100  $\mu$ M. Likewise, ortho or meta substitution in the phenyl ring (analogs **3-5**) or extending the linker length (analog **6**) drastically decreased the potency. A similar trend was observed for analogs **7-23** which have drastic structural modifications in the form of bulkier groups, amides, or acids, possibly due to disruption of the three-dimensional orientation of the molecules that can no longer fit in the binding pocket. We performed only limited modifications in the *N*-phenyl region. Gratifyingly, introducing a *p*-methyl to the *N*-phenyl ring (analog **1**), slightly improved the potency with an  $IC_{50} = 0.27 \mu$ M. In summary, we observed minor SAR effects and our limited efforts on this chemotype indicated that major structural changes were not well tolerated.

### 3.7 Computational Docking of h15-LOX-2 Inhibitors

In order to predict binding modes of **327069**, **327206**, **327186**, **545091** and **536924**, we docked them using the method described above, and docking poses are shown in Figure 2 and Table 5. The inhibitors bind in the U-shaped active site, with the heterocyclic ring occupying the pocket near the metal ion and both aromatic rings filling the hydrophobic pockets on either side of the heterocycle. For all inhibitors, except **536924** and **545091**, the central heterocyclic ring makes a pi-stacking interaction with the side chain of His373 (Figure 2). The binding affinities predicted by the docking score (Glide SP) or MM-GBSA energy (Table 5) correlate weakly with the narrow range of experimental  $IC_{50}$  values, with the inhibitors **327069**, **327206** and **327186** ranking marginally better than **545091** and **536924**.<sup>20</sup> These docking poses demonstrate that the heterocyclic ring and the positions of the substituents attached to the heterocyclic ring are different among these compounds. Substituents attached at these carbon and nitrogen atoms, as found in **327069**, **327206** and **327186**, might facilitate the favorable pi-stacking interaction for these compounds with F438.

### 3.8 Co-Structure of h15-LOX-2 and Inhibitor

The original crystallization condition of h15-LOX-2 required a detergent for high-resolution structure determination.<sup>8</sup> The substrate-mimicking, competitive-inhibitor detergent, octyltetraethylene glycol ether (C8E4), was bound in the active site described as a U-shaped channel.<sup>32</sup> An additional detergent molecule was revealed next to the catalytic domain near helix- $\alpha$ 2 (H $\alpha$ 2); it mediates crystal contacts. Attempts at utilizing these conditions for co-inhibitor structural studies were fruitless due to the requirement of the C8E4 detergent. New crystallization conditions were screened for a loop mutant of 15-lipoxygenase-2 (h15-LOX-2 LM), with amino acid residues 73-79 being deleted (PPVLPLL).<sup>33</sup> In the structure of the wildtype enzyme the hydrophobic loop projects from the  $\beta$ -barrel domain and hinders access to the active site of a neighboring promoter in the crystal lattice. Data suggest that peripheral insertion of this loop into the bilayer is the primary membrane-binding determinant for  $Ca^{2+}$ -signaling and targeting.<sup>33</sup> A cocktail of inhibitors **545091** and **536924** was used in the crystallization trials of h15-LOX-2 LM substituted with  $Mn^{2+}$ . This h15-LOX-2 LM substituted with  $Mn^{2+}$  showed no kinetic activity, as despite the fact that the metal coordination is equivalent in the substituted enzymes, the enzymes are inactive. Crystals

grew in our high-throughput screening (HTS) effort in conditions of 20% DMSO and 20% Jeffamine M-2070. Rod-shaped crystals directly from the HTS condition were flash-frozen and x-ray diffraction data were collected. The protein crystallized in space group C2 and data was collected to 2.4-Å resolution (Supporting Information, Table S1). Two monomers were positioned in the asymmetric unit of the search model h15-LOX-2 WT (4nre.pdb). According to the macromolecular interface tool PISA (Proteins, Interfaces, Structures and Assemblies), this interface is significant and could represent the dimer observed in size-exclusion chromatography.<sup>34</sup>

Additional electron density lFo-FcI near the active site metal was resolved after subsequent refinement (Supporting Information, Figure S12). The different inhibitors were modeled and refined in parallel refinements in the density near the active site metal. However, we are unable to unambiguously identify which inhibitor(s) is(are) present. Real-space correlation coefficients for inhibitor **536924** (0.88 CC and 0.89 CC) in both chains correlate to a higher degree versus inhibitor **545091** (0.79 CC and 0.82 CC). We can, however, unambiguously state that the inhibitors bind in the U-shaped channel and do not directly interact with the active-site metal (Figure 3). Additionally, a water molecule that occupies the open sixth position of the octahedral-coordinated Fe<sup>2+</sup> in the wildtype structure was observed in chain A of the crystal structure of the Mn<sup>2+</sup>-substituted h15-LOX-2 LM (Supporting Information, Figure S13). When inhibitor **536924** is placed in the electron density near the metal, the sulfur of the inhibitor forms an H-bond with the Mn<sup>2+</sup>-coordinated water and His 373. All other potential interactions of inhibitors in the crystal structures share only van der Waal contacts in the U-shaped pocket defined by Ile 412, Phe 365, Thr 431, and Leu 420, which positions the targeted pentadiene of AA for hydrogen atom abstraction. The crystal structure validates many key findings of the docking experiments including water-mediated binding of the inhibitor to the metal coordination sphere near the imidazole heterocycle, and the aromatic structures of the inhibitors positioned on opposite ends of the U-shaped channel. The minimal differences of the atomic positions of amino acids in the original wild-type structure of h15-LOX-2 bound to the detergent C8E4 and our new structure of h15-LOX-2 LM co-crystallized with a cocktail of inhibitors (7laf.pdb) further validate and justify the *in silico* rigid-body docking strategy performed.

### 3.9 Hydrogen/Deuterium Exchange Mass Spectrometry of h15-LOX-2

Hydrogen/deuterium exchange mass spectrometry (HDX-MS) is often utilized to assess the effects of binding small molecule effectors, regulators, and inhibitors on protein conformational flexibility.<sup>29, 35-39</sup> Therefore, it offers an incisive high-throughput technique, complementary to the high-resolution X-ray crystal structures solved with inhibitors bound, to screen inhibitors and to resolve their impact on protein structure and flexibility. In the specific case of lipoxygenases, allosteric effectors and substrates have been shown to influence the HDX properties of both soybean lipoxygenase-1 (SLO-1)<sup>40</sup> and human 15-LOX-2.<sup>41</sup>

Herein, we sought to examine the impact of the isozyme selective inhibitors, **536924** which was characterized previously,<sup>20</sup> and **327069** which is described in this report. Tandem MS analysis of pepsin-generated peptides of 15-LOX-2 identified 242 peptides corresponding

to 94% coverage of the primary sequence. This represents a significant increase in primary sequence coverage from the previous report of 72%.<sup>41</sup> For data reduction purposes, 44 non-overlapping peptides, ranging from 5 to 25 amino acids (average length, 12), were selected for HDX-MS analysis. The peptide list was well covered over all 10 time points, ranging from 10 s to 2 h, and identical for samples prepared with inhibitors.

The percent exchange at 2 h for samples of h15-LOX-2 alone is mapped onto the crystal structure of 15-LOX-2<sup>8</sup> (Figure 4A) that was solved with a substrate mimic, C8E4, in the active site. The general trend in this HDX heat map is comparable to that reported from the Armstrong lab.<sup>41</sup> Of note is the exchange behavior of helix- $\alpha$ 2, a peptide which restricts the substrate entrance portal and whose flexibility has been implicated to play an important regulatory role in substrate binding in LOXs.<sup>20, 40, 42, 43</sup>

Peptide 184-191 (and its overlapping counterparts) is located in the central region of helix  $\alpha$ 2 and flanked by peptides 173-184 (Figure 4B, chartreuse) and 192-206 (Figure 4B, salmon). All three peptides are highly exchanged ( ~ 80%) at 2 h (Figure 4A and 4B). Considering the variability in protein handling, mass spectrometry instrumentation used, and potential differences in buffer preparation, the exchange properties of this helix  $\alpha$ 2 reported in Droege *et al.*<sup>41</sup> and herein are nearly identical (see Supporting Information, Figure S14A). Further, to corroborate our h15-LOX-2 HDX properties, we conducted HDX-MS of h15-LOX-2 isolated from insect cell (SF9) cultures and compared them to the HDX-MS results for h15-LOX-2 isolated from *E. coli* cultures. Exchange properties are nearly superimposable including helix  $\alpha$ 2 (Figure S14B). The observed elevated exchange behavior for a crystallographically resolved alpha-helical peptide is comparable to that described for the model 15-lipoxygenase from plants, SLO-1 (Figure S15).<sup>30, 40</sup>

One notable distinction between h15-LOX-2 and SLO-1 is the general increase in the exchange of the N-terminal PLAT domain with an average 10% higher overall extent of exchange for 15-LOX-2 (Figure S15). In addition, the linker peptide between the PLAT and catalytic domains, 117-134, in h15-LOX-2 exhibits a significantly higher exchange (87% at 2 h) compared to the corresponding peptide in SLO-1 of *ca.* 45 % (residues 137-160). The trend in these HDX properties of the PLAT domain is consistent with the previously reported small-angle X-ray scattering (SAXS) experiments. SAXS data of rabbit 15-LOX-1 suggested high mobility of the PLAT domain, supporting a ‘rocking’ motion that has been proposed to play a role in membrane binding.<sup>44, 45</sup> Conversely, SAXS analysis of SLO-1 indicates no significant mobility of the PLAT domain.<sup>46</sup>

### 3.10 Impact of isozyme-selective inhibitors on h15-LOX-2 Hydrogen/Deuterium Exchange properties

The addition of substrate arachidonic acid (AA) to h15-LOX-2 was previously found to decrease the exchange behavior of peptide 185-191 (helix  $\alpha$ 2) at early time points (15-120 s) by as much as 20%.<sup>41</sup> This was accompanied by a modest impact on the exchange percentage at the arched helix that runs nearly parallel to helix  $\alpha$ 2 and lines the substrate-binding site. This leads to the question of whether the inhibitors described herein might influence regional protein flexibility of 15-LOX-2 and, if so, to what extent.



For the current HDX study of h15-LOX-2, two inhibitors were selected, **536924** and **327069**, that represented the two different chemotypes of this study. In the presence of saturating concentration (20  $\mu\text{M}$ ) of **327069**, two non-overlapping h15-LOX-2 peptides (173-184 and 184-191) were associated with a significant reduction in exchange by as much as 20% at short time scales (< 10 min). From the bi-exponential fits of the time-dependent HDX traces (Figure 4C), the average rate constants for these peptides were found to be 2- and 4-times slower in the presence of **327069**. These trends were validated from analysis of overlapping peptides in this region (Figure S16). This behavior is consistent with a rigidification of regional protein motions and is the canonical HDX behavior reported for protein inhibitors (see refs<sup>47-50</sup> for examples). The rigidification of helix  $\alpha 2$  in the presence of **327069** was also similar to the HDX behavior previously characterized at short time scales for the presence of AA.<sup>41</sup> Conversely, within the dynamic range of the experiment employed, HDX samples of h15-LOX-2 prepared with **536924** showed no significant exchange differences to samples with 15-LOX-2 alone (*cf.* Figure 4C, black and gray traces). The difference in HDX behavior observed here for the two different h15-LOX-2 inhibitors can be attributed to the nearly 10-fold enhanced inhibition of **327069** ( $\text{IC}_{50} = 0.34 \mu\text{M}$ ) over **536924** ( $\text{IC}_{50} = 3.1 \mu\text{M}$ ). The observation that the more potent inhibitor resulted in the structural rigidification of h15-LOX-2 helix  $\alpha 2$  underscores the utility of HDX-MS as a powerful, high-throughput method for screening h15-LOX-2 inhibitors.

Droege *et al.* previously reported notable decreased HDX-MS behavior for h15-LOX-2 peptides in the PLAT domain, namely 45-52, 54-66, and 67-86 with the addition of the AA substrate.<sup>41</sup> However, from our data even under saturating inhibitor concentrations, there is no significant effect on the apparent HDX rate in this region between the samples in the presence and absence of either inhibitor (Supporting Information, HDX traces). Note that at long time points, the inhibitors cause a slight increase in the extent of exchange, including peptide 45-53. Because this is only observed at longer time points, we attribute this effect to a possible regional dependent destabilization of the protein structure in the presence of the inhibitors.

This distinction between the exchange behavior reported for AA and that described for the inhibitors described herein could be catalytically significant. Note that during the 15-120 second exchange experiment with AA,<sup>41</sup> the substrate will be converted to 15-HpETE. While not fully resolved for h15-LOX-2, conformational changes are expected to accompany substrate binding, turnover, and product release.<sup>51</sup> Further, AA could potentially bind at an allosteric site in h15-LOX-2 and elicit altered protein conformational ensembles. The substrate selectivity of h15-LOX-2 has been shown to be influenced by allosteric effectors, including 13*S*-HODE, an enzymatic product from the reaction of h15-LOX-1 with linoleic acid.<sup>52</sup> Allosteric effects in the HDX behavior have also been detected in the PLAT domain of SLO-1 when using the SLO-1 allosteric effector, oleyl sulfate.<sup>40</sup> Future HDX-MS studies will be aimed at resolving the effects of the interactions of selective allosteric modulators that target h15-LOX-2.

### 3.11 Inhibition of h15-LOX-2 in HEK293T cells

A key aspect of any inhibitor that will be used as a tool to investigate the biological relevancy of h15-LOX-2 is its efficacy in a cellular model. Currently, there are no potent/specific inhibitors against h15-LOX-2 which are effective in the cellular milieu. Our h15-LOX-2 inhibitors of this work and our previous work,<sup>20</sup> were therefore tested in HEK293T cells expressing h15-LOX-2 to inhibit LOX activity and reduce 15-HETE production. The majority of these inhibitors, **327069**, **327206** and **536924**, demonstrated EC<sub>50</sub> values of approximately 1 μM (Table 6, Supporting Information, Figure S17), which is consistent with their *in vitro* IC<sub>50</sub> values (Table 2). **327186**, however, manifested weaker potency, with an approximate EC<sub>50</sub> of *ca.* 30 μM. It is unclear why **327186** is less potent, but it could be due to increased cellular inactivation or decreased cell penetration. Nonetheless, these data demonstrate that this class of inhibitors can penetrate the cell and inhibit the oxygenation of free, exogenous AA. Additionally, these inhibitors were non-toxic, since cells continued to grow at the same rate as their DMSO controls after treatment with 10 μM of all four inhibitors, confirming them as viable *ex vivo* tools for examining the activity of h15-LOX-2.

## Conclusions

In summary, we have discovered three inhibitors of h15-LOX-2, **327069**, **327186**, and **327206**, that are potent and highly selective against h15-LOX-2 over other human LOX isozymes. They are mixed-type inhibitors and non-reductive, similar to our previously published h15-LOX-2 inhibitors, **545091** and **536924**. Importantly, they all perform as potent inhibitors in our HEK293 cell-based assay, indicating their novelty as useful chemical tools for biological activity assays and their potential to help further delineate the role of h15-LOX-2 in particular human disease models. In addition, our structural and computational data indicate that all five inhibitors bind in the U-shaped channel in similar binding poses (Figure 5). The HDX results support a similar binding mode between **536924** and **327069**, with the latter restricting protein motion of helix-α2 more robustly, consistent with its greater potency. Given these results, we designed, docked, and synthesized novel inhibitors and confirmed our binding mode hypothesis. As such, we have discovered a suite of similar chemotypes that target h15-LOX-2 both *in vitro* and *ex vivo* and we are further developing them as h15-LOX-2 therapeutic agents.

## Supplementary Material

Refer to Web version on PubMed Central for supplementary material.

## Acknowledgements:

This work was funded in part by grants to T.R.H. (NIH, GM105671 and Molecular Libraries Initiative, MH081283), to A.Y., A.J. and A.S. (National Center for Advancing Translational Sciences and the Molecular Libraries Initiative, NIH), to M.E.N. (nos. NIH HL107887 and AHA 16GRNT31000010, and the NIH P50AT002776 seed grant, and the Louisiana Governor's Biotechnology Initiative). Preliminary X-ray data were collected at the Center for Advanced Microstructures and Devices (Baton Rouge). We thank the staff at the Center for Advanced Microstructures and Devices for screening and data collection of macromolecular crystals at the Protein Crystallography beamline. The work is based on research conducted at the Northeastern Collaborative Access Team beamlines, which are funded by the National Institute of General Medical Sciences from the National Institutes of Health (grant no. P30 GM124165). The Eiger 16M detector on 24-ID-E beam line is funded by a NIH-ORIP HEI grant (no. S10OD021527). This research used resources of the Advanced Photon Source, a

US Department of Energy (DOE) Office of Science User Facility operated for the DOE Office of Science by Argonne National Laboratory under contract no. DE-AC02-06CH11357. A.T.I. acknowledges NIH support (1S10 OD020062-01).

## References

- [1]. Klinman JP (2007) How Do Enzymes Activate Oxygen without Inactivating Themselves, *Accounts of Chemical Research* 40, 325–333. [PubMed: 17474709]
- [2]. Dobrian Anca D.a, L. DC, Cole Banumathi K.b, Taylor-Fishwick David A.b., and Chakrabarti Swarup K.b, a. N. JL (2011) Functional and Pathological Roles of the 12- and 15-lipoxygenases, *Prog Lipid Res* 50, 115–131. [PubMed: 20970452]
- [3]. Funk CD, Chen XS, Johnson EN, and Zhao L (2002) Lipoxygenase genes and their targeted disruption, *Prostaglandins & other lipid mediators* 68-69, 303–312. [PubMed: 12432925]
- [4]. Funk CD (2006) Lipoxygenase pathways as mediators of early inflammatory events in atherosclerosis, *Arteriosclerosis, thrombosis, and vascular biology* 26, 1204–1206.
- [5]. Brash AR, Boeglin WE, and Chang MS (1997) Discovery of a second 15S-lipoxygenase in humans, *Proc Natl Acad Sci U S A* 94, 6148–6152. [PubMed: 9177185]
- [6]. Jisaka M, Kim RB, Boeglin WE, Nanney LB, and Brash AR (1997) Molecular cloning and functional expression of a phorbol ester-inducible 8S-lipoxygenase from mouse skin, *J Biol Chem* 272, 24410–24416. [PubMed: 9305900]
- [7]. Hulten LM, Olson FJ, Aberg H, Carlsson J, Karlstrom L, Boren J, Fagerberg B, and Wiklund O (2010) 15-Lipoxygenase-2 is expressed in macrophages in human carotid plaques and regulated by hypoxia-inducible factor-1alpha, *Eur J Clin Invest* 40, 11–17. [PubMed: 19912316]
- [8]. Kobe MJ, Neau DB, Mitchell CE, Bartlett SG, and Newcomer ME (2014) The structure of human 15-lipoxygenase-2 with a substrate mimic, *J Biol Chem* 289, 8562–8569. [PubMed: 24497644]
- [9]. Danielsson KN, Rydberg EK, Ingelsten M, Akyurek LM, Jirholt P, Ullstrom C, Forsberg GB, Boren J, Wiklund O, and Hulten LM (2008) 15-Lipoxygenase-2 expression in human macrophages induces chemokine secretion and T cell migration, *Atherosclerosis* 199, 34–40. [PubMed: 18067895]
- [10]. Rydberg EK, Krettek A, Ullstrom C, Ekstrom K, Svensson PA, Carlsson LM, Jonsson-Rylander AC, Hansson GI, McPheat W, Wiklund O, Ohlsson BG, and Hulten LM (2004) Hypoxia increases LDL oxidation and expression of 15-lipoxygenase-2 in human macrophages, *Arteriosclerosis, thrombosis, and vascular biology* 24, 2040–2045.
- [11]. Hersberger M (2010) Potential role of the lipoxygenase derived lipid mediators in atherosclerosis: leukotrienes, lipoxins and resolvins, *Clin Chem Lab Med* 48, 1063–1073. [PubMed: 20441482]
- [12]. Gertow K, Nobili E, Folkersen L, Newman JW, Pedersen TL, Ekstrand J, Swedenborg J, Kuhn H, Wheelock CE, Hansson GK, Hedin U, Haeggstrom JZ, and Gabrielsen A (2011) 12- and 15-lipoxygenases in human carotid atherosclerotic lesions: associations with cerebrovascular symptoms, *Atherosclerosis* 215, 411–416. [PubMed: 21316676]
- [13]. Magnusson LU, Lundqvist A, Carlsson MN, Skalen K, Levin M, Wiklund O, Boren J, and Hulten LM (2012) Arachidonate 15-lipoxygenase type B knockdown leads to reduced lipid accumulation and inflammation in atherosclerosis, *PLoS One* 7, e43142. [PubMed: 22912809]
- [14]. Wuest SJ, Cruet M, Gemperle C, Loretz C, and Hersberger M (2012) Expression and regulation of 12/15-lipoxygenases in human primary macrophages, *Atherosclerosis* 225, 121–127. [PubMed: 22980500]
- [15]. Kotla S, Singh NK, Heckle MR, Tigyi GJ, and Rao GN (2013) The transcription factor CREB enhances interleukin-17A production and inflammation in a mouse model of atherosclerosis, *Sci Signal* 6, ra83. [PubMed: 24045154]
- [16]. Ringholz FC, Buchanan PJ, Clarke DT, Millar RG, McDermott M, Linnane B, Harvey BJ, McNally P, and Urbach V (2014) Reduced 15-lipoxygenase 2 and lipoxin A4/leukotriene B4 ratio in children with cystic fibrosis, *Eur Respir J* 44, 394–404. [PubMed: 24696116]
- [17]. Wenzel SE, Tyurina YY, Zhao J, St Croix CM, Dar HH, Mao G, Tyurin VA, Anthonyamuthu TS, Kapralov AA, Amoscato AA, Mikulska-Ruminska K, Shrivastava IH, Kenny EM, Yang Q, Rosenbaum JC, Sparvero LJ, Emler DR, Wen X, Minami Y, Qu F, Watkins SC, Holman TR, VanDemark AP, Kellum JA, Bahar I, Bayir H, and Kagan VE (2017) PEBP1 Wardens

Ferroptosis by Enabling Lipoxygenase Generation of Lipid Death Signals, *Cell* 171, 628–641 e626. [PubMed: 29053969]

- [18]. Reichert CO, de Freitas FA, Sampaio-Silva J, Rokita-Rosa L, Barros PL, Levy D, and Bydlowski SP (2020) Ferroptosis Mechanisms Involved in Neurodegenerative Diseases, *Int J Mol Sci* 21.
- [19]. Vasquez-Martinez Y, Ohri RV, Kenyon V, Holman TR, and Sepulveda-Boza S (2007) Structure-activity relationship studies of flavonoids as potent inhibitors of human platelet 12-hLO, reticulocyte 15-hLO-1, and prostate epithelial 15-hLO-2, *Bioorganic & Medicinal Chemistry* 15, 7408–7425. [PubMed: 17869117]
- [20]. Jameson JB 2nd, Kantz A, Schultz L, Kalyanaraman C, Jacobson MP, Maloney DJ, Jadhav A, Simeonov A, and Holman TR (2014) A high throughput screen identifies potent and selective inhibitors to human epithelial 15-lipoxygenase-2, *PLoS One* 9, e104094. [PubMed: 25111178]
- [21]. Robinson SJ, Hoobler EK, Riener M, Loveridge ST, Tenney K, Valeriote FA, Holman TR, and Crews P (2009) Using enzyme assays to evaluate the structure and bioactivity of sponge-derived meroterpenes, *Journal of Natural Products* 72, 1857–1863. [PubMed: 19848434]
- [22]. Amagata T, Whitman S, Johnson TA, Stessman CC, Loo CP, Lobkovsky E, Clardy J, Crews P, and Holman TR (2003) Exploring sponge-derived terpenoids for their potency and selectivity against 12-human, 15-human, and 15-soybean lipoxygenases, *J Nat Prod* 66, 230–235. [PubMed: 12608855]
- [23]. Bender G, Schexnaydre EE, Murphy RC, Uhlson C, and Newcomer ME (2016) Membrane-dependent Activities of Human 15-LOX-2 and Its Murine Counterpart: Implications for Murine Models of Atherosclerosis, *J Biol Chem* 291, 19413–19424. [PubMed: 27435673]
- [24]. Hoobler EK H. C; Holman TR . (2013) Pseudoperoxidase Investigations of Hydroperoxides and Inhibitors with Human Lipoxygenases, *Bioorg Med Chem* 21, 3894–3899. [PubMed: 23669189]
- [25]. Rai G, Kenyon V, Jadhav A, Schultz L, Armstrong M, Jameson JB, Hoobler E, Leister W, Simeonov A, Holman TR, and Maloney DJ (2010) Discovery of potent and selective inhibitors of human reticulocyte 15-lipoxygenase-1, *J Med Chem* 53, 7392–7404. [PubMed: 20866075]
- [26]. Karplus PA, and Diederichs K (2015) Assessing and maximizing data quality in macromolecular crystallography, *Curr Opin Struct Biol* 34, 60–68. [PubMed: 26209821]
- [27]. Adams PD, Afonine PV, Bunkoczi G, Chen VB, Echols N, Headd JJ, Hung LW, Jain S, Kapral GJ, Grosse Kunstleve RW, McCoy AJ, Moriarty NW, Oeffner RD, Read RJ, Richardson DC, Richardson JS, Terwilliger TC, and Zwart PH (2011) The Phenix software for automated determination of macromolecular structures, *Methods* 55, 94–106. [PubMed: 21821126]
- [28]. Pascal BD, Willis S, Lauer JL, Landgraf RR, West GM, Marciano D, Novick S, Goswami D, Chalmers MJ, and Griffin PR (2012) HDX Workbench: software for the analysis of H/D exchange MS data, *J. Am. Soc. Mass Spectrom* 23, 1512–1521. [PubMed: 22692830]
- [29]. Hoofnagle AN, Resing KA, and Ahn NG (2003) Protein analysis by hydrogen exchange mass spectrometry, *Annu Rev Biophys Biomol Struct* 32, 1–25. [PubMed: 12598366]
- [30]. Offenbacher AR, Hu S, Poss EM, Carr CAM, Scouras AD, Prigozhin DM, Iavarone AT, Palla A, Alber T, Fraser JS, and Klinman JP (2017) Hydrogen-deuterium exchange of lipoxygenase uncovers a relationship between distal, solvent exposed protein motions and the thermal activation barrier for catalytic proton-coupled electron tunneling, *ACS Cent. Sci* 3, 570–579. [PubMed: 28691068]
- [31]. Yeung J, Tourdot BE, Adili R, Green AR, Freedman CJ, Fernandez-Perez P, Yu J, Holman TR, and Holinstat M (2016) 12(S)-HETrE, a 12-Lipoxygenase Oxylin of Dihomo-gamma-Linolenic Acid, Inhibits Thrombosis via Galphas Signaling in Platelets, Arteriosclerosis, thrombosis, and vascular biology 36, 2068–2077.
- [32]. Newcomer ME, and Brash AR (2015) The structural basis for specificity in lipoxygenase catalysis, *Protein Sci* 24, 298–309. [PubMed: 25524168]
- [33]. Neau DB, Gilbert NC, Bartlett SG, Boeglin W, Brash AR, and Newcomer ME (2009) The 1.85 Å structure of an 8R-lipoxygenase suggests a general model for lipoxygenase product specificity, *Biochemistry* 48, 7906–7915. [PubMed: 19594169]
- [34]. Schlee S, Straub K, Schwab T, Kinateder T, Merkl R, and Sterner R (2019) Prediction of quaternary structure by analysis of hot spot residues in protein-protein interfaces: the case of anthranilate phosphoribosyltransferases, *Proteins* 87, 815–825. [PubMed: 31134642]

- [35]. Marcisin SR, and Engen JR (2010) Hydrogen exchange mass spectrometry: what is it and what can it tell us?, *Anal. Bioanal. Chem* 397, 967–972. [PubMed: 20195578]
- [36]. Chalmers MJ, Busby SA, Pascal BD, West GM, and Griffin PR (2014) Differential hydrogen/deuterium exchange mass spectrometry analysis of protein-ligand interactions, *Expert Rev. Proteomics* 8, 43–59.
- [37]. Wei H, Mo J, Tao L, Russell RJ, Tymiak AA, Chen G, Jacob RE, and Engen JR (2014) Hydrogen/deuterium exchange mass spectrometry for probing higher order therapeutics: methodology and applications, *Drug Discov. Today* 19, 95–102. [PubMed: 23928097]
- [38]. Pirrone GF, Jacob RE, and Engen JR (2015) Applications of hydrogen/deuterium exchange MS from 2012 to 2014, *Anal. Chem* 87, 99–118. [PubMed: 25398026]
- [39]. Masson GR, Jenkins ML, and Burke JE (2017) An overview of hydrogen deuterium exchange mass spectrometry (HDX-MS) in drug discovery, *Expert Opin. Drug Discov* 12, 981–994. [PubMed: 28770632]
- [40]. Offenbacher AR, Iavarone AT, and Klinman JP (2018) Hydrogen-deuterium exchange reveals long-range dynamical allostery in soybean lipoxygenase, *J. Biol. Chem* 293, 1138–1148. [PubMed: 29191828]
- [41]. Droege KD, Keithly ME, Sanders CR, Armstrong RN, and Thompson MK (2017) Structural dynamics of 15-lipoxygenase-2 via hydrogen-deuterium exchange, *Biochemistry* 56, 5065–5074. [PubMed: 28809482]
- [42]. Gilbert NC, Gerstmeier J, Schexnaydre EE, Borner F, Garscha U, Neau DB, Werz O, and Newcomer ME (2020) Structural and mechanistic insights into 5-lipoxygenase inhibition by natural products, *Nat. Chem. Biol* 16, 783–790. [PubMed: 32393899]
- [43]. Offenbacher AR, and Holman TR (2020) Fatty acid allosteric regulation of C-H activation in plant and animal lipoxygenases, *Molecules* 25, 3374.
- [44]. Hammel M, Walther M, Prassl R, and Kuhn H (2004) Structural flexibility of the N-terminal beta-barrel domain of 15-lipoxygenase-1 probed by small angle X-ray scattering. Functional consequences for activity regulation and membrane binding, *J Mol Biol* 343, 917–929. [PubMed: 15476810]
- [45]. Shang W, Ivanov I, Svergun DI, Borbulevych OY, Aleem AM, Stehling S, Jankun J, Kuhn H, and Skrzypczak-Jankun E (2011) Probing dimerization and structural flexibility of mammalian lipoxygenases by small-angle X-ray scattering, *J Mol Biol* 409, 654–668. [PubMed: 21530540]
- [46]. Dainese E, Sabatucci A, van Zadelhoff G, Angelucci CB, Vachette P, Veldink GA, Agro AF, and Maccarrone M (2005) Structural stability of soybean lipoxygenase-1 in solution as probed by small angle X-ray scattering, *J Mol Biol* 349, 143–152. [PubMed: 15876374]
- [47]. Cao J, Burke JE, and Dennis EA (2013) Using hydrogen/deuterium exchange mass spectrometry to define the specific interactions of the phospholipase A2 superfamily with lipid substrates, inhibitors, and membranes, *J. Biol. Chem* 288, 1806–1813. [PubMed: 23209293]
- [48]. Konermann L, Pan J, and Liu Y-H (2011) Hydrogen exchange mass spectrometry for studying protein structure and dynamics, *Chem. Soc. Rev* 40, 1224–1234. [PubMed: 21173980]
- [49]. Sherry K, Schaper Bergman ET, Beno BR, Huang RY-C, Deyanova E, Chen G, and Gross ML (2019) Hydrogen-deuterium exchange and hydroxyl radical footprinting for mapping hydrophobic interactions of human bromodomain with a small molecule inhibitor, *J. Am. Soc. Mass Spectrom* 30, 2795–2804. [PubMed: 31720974]
- [50]. Pegram LM, Liddle JC, Xiao X, Hoh M, Rudolph J, Iverson DB, Vigers GP, Smith D, Zhang H, Wang W, Moffat JG, and Ahn NG (2019) Activation loop dynamics are controlled by conformation-selective inhibitors of ERK2, *Proc. Natl. Acad. Sci. U.S.A* 116, 15463–15468. [PubMed: 31311868]
- [51]. Ramachandran S, Richards-Suchek TJ, Skrzypczak-Jankun E, Wheelock MJ, and Funk MO Jr. (1995) Catalysis sensitive conformational changes in soybean lipoxygenase revealed by limited proteolysis and monoclonal antibody experiments, *Biochemistry* 34, 14868–14873. [PubMed: 7578097]
- [52]. Joshi N, Hoobler EK, Perry S, Diaz G, Fox B, and Holman TR (2013) Kinetic and structural investigations into the allosteric and pH effect on the substrate specificity of human epithelial 15-lipoxygenase-2, *Biochemistry* 52, 8026–8035. [PubMed: 24171444]

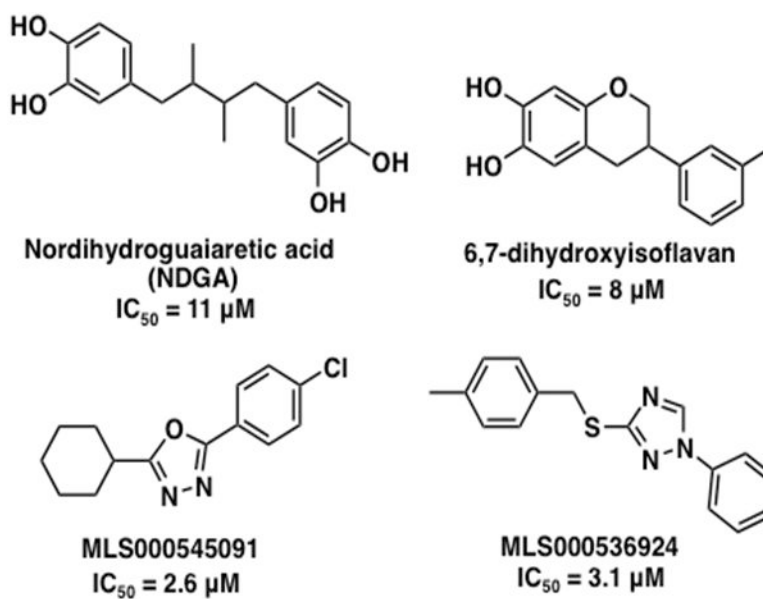


**Figure 1.**  
Structures of known h15-LOX-2 inhibitors.

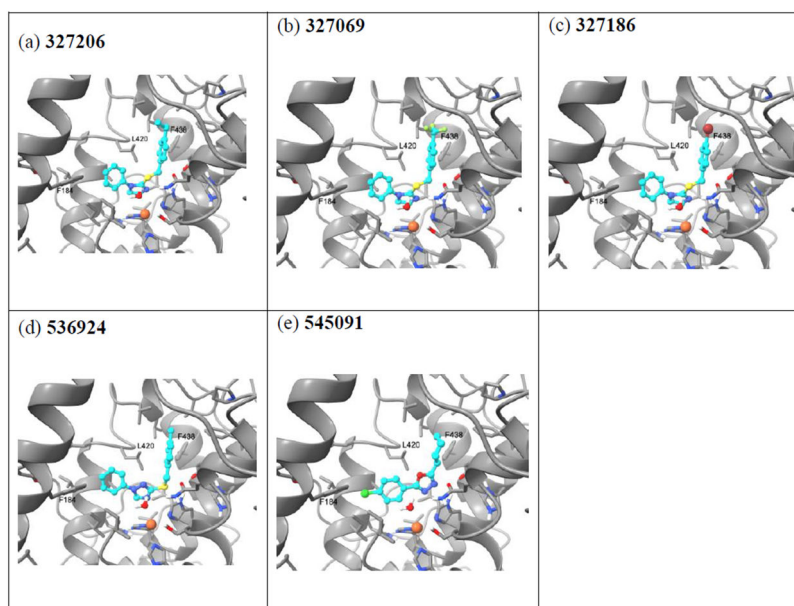


**Figure 2.** Docking pose of ligands bound to h15-LOX-2 (a) **327206**, (b) **327069**, (c) **327186**, (d) **536924**, (e) **545091**. Carbon atoms of the ligands are shown in cyan color and the protein is shown in grey color. Nitrogen, oxygen, sulfur, fluorine, bromine and hydrogen atoms are shown in blue, red, yellow, green, brown and white colors respectively and the metal ion is shown in orange color.

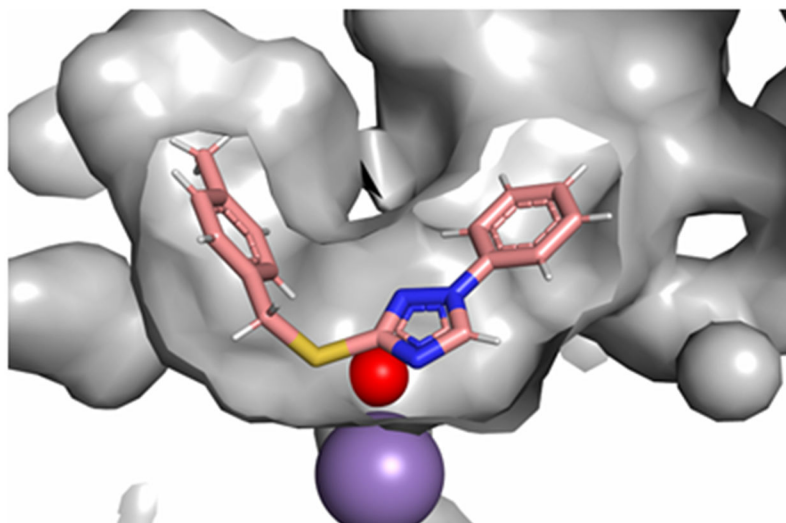


**Figure 3. Inhibitor 536924 in the U-shaped channel.**

Surface rendering in the cavities and pockets only mode from Pymol of chain A of the 15-LOX-2 LM structure (7laf.pdb) is shown in grey. The  $Mn^{2+}$  is shown as purple sphere and water molecule as red sphere. Inhibitor 536924 (C, pink) binds in the U-shaped channel and interacts with the water that coordinates the 6<sup>th</sup> position of the metal.



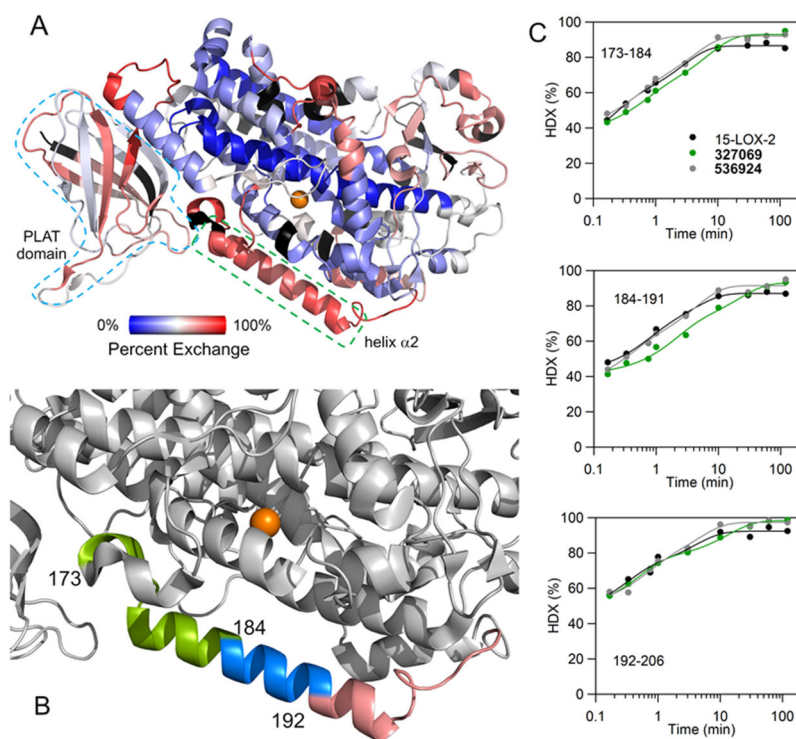


**Figure 4.** HDX-MS properties of 15-LOX-2 isozyme-specific inhibitors. (A) HDX-MS behavior at 2 h and 25 °C of h15-LOX-2 peptides in the absence of an inhibitor is mapped onto the crystal structure (PDB entry, 4NRE). The coloring is defined by the spectrum bar. Black coloring represents uncovered regions. The PLAT domain is highlighted by cyan outline and the helix  $\alpha$ 2 is highlighted by the green box. (B, C) presents the impact of isozyme selective inhibitors, **536924**<sup>20</sup> and **327069**, on the HDX-MS properties of 15-LOX-2. The effect is localized to the helix  $\alpha$ 2 of 15-LOX-2 and the peptides are colored as follows: chartreuse, 173-184; marine, 184-191; and salmon, 192-206. Additionally, overlapping peptides are presented in the SI HDX traces pdf.

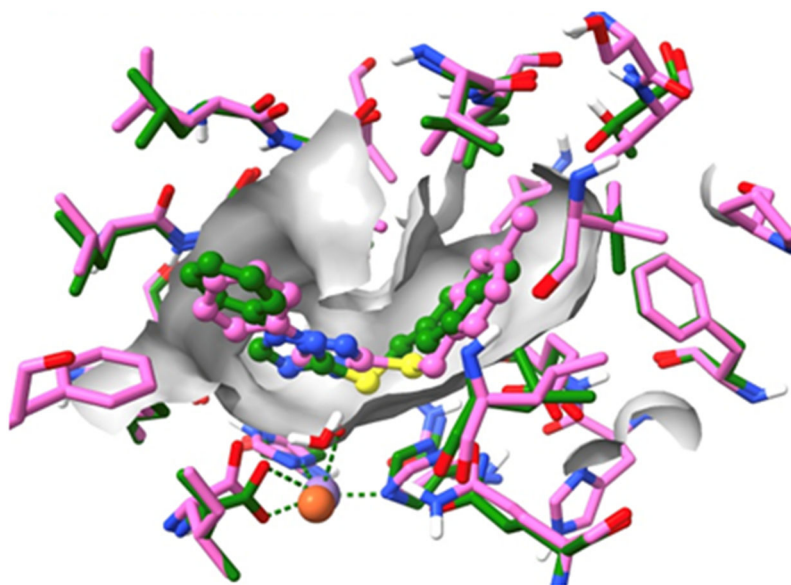
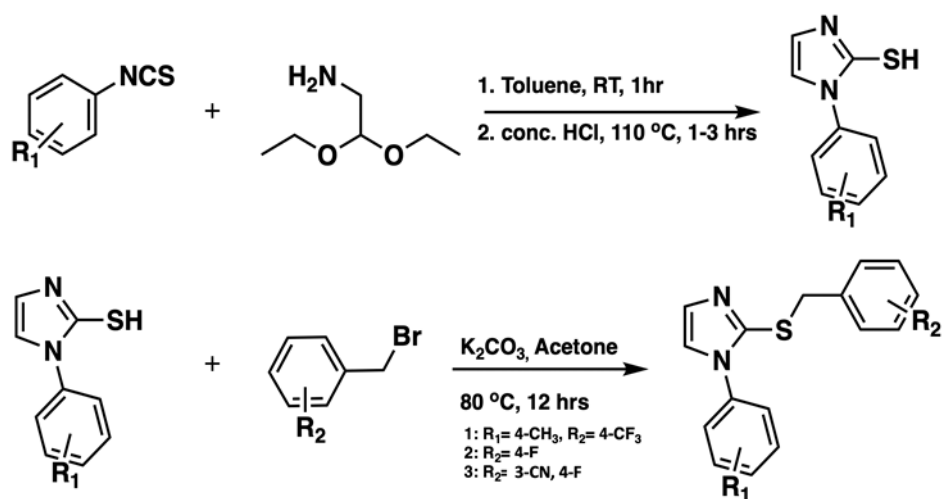


**Figure 5.** Docking comparison of **536924** bound to h15-LOX-2, crystal structure (green) and docking model (pink).



**Scheme 1.**  
Synthesis of h15-LOX-2 inhibitor derivatives, **1-3**.

**Table 1.**

Real-space correlation coefficients and occupancies.

Ligand	Real-space correlation coefficients	Occupancy
<b>536924</b>	(chain A) 0.89 (chain B) 0.89	(chain A) 0.65 (chain B) 0.70
<b>536924</b> (flipped)	(chain A) 0.83 (chain B) 0.89	(chain A) 0.68 (chain B) 0.75
<b>545091</b>	(chain A) 0.79 (chain B) 0.82	(chain A) 0.68 (chain B) 0.73
<b>545091</b> (flipped)	(chain A) 0.75 (chain B) 0.78	(chain A) 0.66 (chain B) 0.70

Author Manuscript

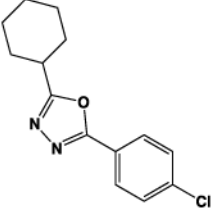
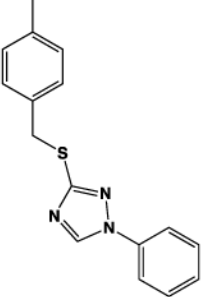
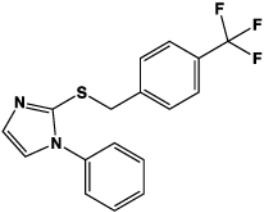
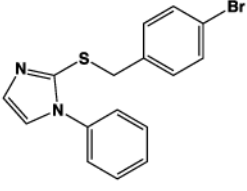
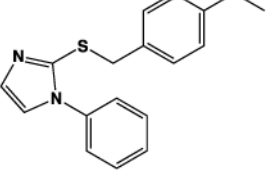
Author Manuscript

Author Manuscript

Author Manuscript

**Table 2.**

IC<sub>50</sub> values for the newly discovered inhibitors targeting h15-LOX-2 with error in parentheses. All experiments were conducted in duplicate and with 10 μM AA.

Inhibitor	Structure	IC <sub>50</sub> (μM) (± SD (μM))
MLS000545091* (545091)		2.6 (0.4)
MLS000536924* (536924)		3.1 (0.4)
MLS000327069 (327069)		0.34 (0.05)
MLS000327186 (327186)		0.53 (0.04)
MLS000327206 (327206)		0.87 (0.06)

\* = Previously published in reference 20.

**Table 3.**

The equilibrium constant of dissociation from the catalytic ( $K_{ic}$ ) and secondary ( $K_{iu}$ ) sites extracted from Dixon plots and Dixon replots of h15-LOX-2 and 545091, 536924, 327069, 327186, and 327206.

Inhibitor	$K_{ic}$ ( $\mu\text{M}$ )	$K_{iu}$ ( $\mu\text{M}$ )
545091 <sup>a</sup>	0.90 (0.4)	9.9 (0.7)
536924 <sup>a</sup>	2.5 (0.5) <sup>b</sup>	N/A
327069	0.70 (0.07)	1.2 (0.9)
327186	0.80 (0.05)	4.0 (3)
327206	0.90 (0.04)	3.4 (2)

<sup>a</sup>Previously published<sup>20</sup>.

<sup>b</sup>536924 displayed competitive inhibition.

**Table 4.**

Full IC<sub>50</sub> experiments were performed with h15-LOX-2, while for the other oxygenases the IC<sub>50</sub> values were estimated at 25  $\mu$ M inhibitor concentration. Inhibition that was less than 15% and less than 30% at 25  $\mu$ M are estimated to have IC<sub>50</sub> values of > 100  $\mu$ M and > 50  $\mu$ M, respectively. All experiments were done in duplicate, and all assays were performed with 10  $\mu$ M AA except for the cyclooxygenases which were conducted at 100  $\mu$ M AA. The values are in units of micromolar with error displayed in the parentheses.

Inhibitors	h15- LOX-2	h15- LOX-1	h12- LOX	h5- LOX	m15- LOX-2	COX- 1	COX- 2	Redox
<b>327069</b>	0.34 (0.05)	> 50	> 100	> 100	>50	> 100	> 100	No
<b>327186</b>	0.53 (0.04)	> 50	> 100	> 100	>50	> 100	> 100	No
<b>327206</b>	0.87 (0.06)	> 50	> 100	> 100	>50	> 100	> 100	No

**Table 5.**

Docking scores of h15-LOX-2 ligands docked to h15-LOX-2 crystal structure (pdb id: 4nre).

Compound	Glide SP Docking Score	MM-GBSA Relative binding energy (kcal/mol)	h15-LOX-2 IC <sub>50</sub> (μM)
327069	-8.1	3.23	0.34
327186	-7.8	6.83	0.53
327206	-8.2	12.35	0.87
545091	-7.0	29.76	2.6
536924	-7.7	20.10	3.1

Author Manuscript

Author Manuscript

Author Manuscript

Author Manuscript



**Table 6.**EC<sub>50</sub> values determined in h15-LOX-2/HEK293T cells.

Inhibitor	EC <sub>50</sub> (μM)
536924	0.60 (0.1)
327069	0.75 (0.2)
327186	31 (6)
327206	1.3 (0.3)

Author Manuscript

Author Manuscript

Author Manuscript

Author Manuscript